Progress In Electromagnetics Research C, Vol. 35, 49–61, 2013

PLANAR MICROSTRIP BANDPASS FILTER WITH WIDE DUAL BANDS USING PARALLEL-COUPLED LINES AND STEPPED IMPEDANCE RESONATORS

Jayaseelan Marimuthu*, Amin M. Abbosh, and Bassem Henin

School of ITEE, The University of Queensland, St. Lucia, QLD4072, Australia

Abstract—A dual-band bandpass filter with wide and highly attenuated stopbands is designed using parallel coupled microstrip line (PCML) and stepped-impedance-resonators (SIRs). The proposed filter is composed of a pair of highly coupled PCML-SIR structure and a central resonator using a low impedance rectangular microstrip. Initially, the wide dual-band performance is achieved by creating a transmission zero between those two bands using a tightly coupled PCML-SIR with a suitable impedance ratio. Then, a low impedance resonator is placed between the pair of PCML-SIR to generate multiple resonant frequencies for a broadband performance. The simulated and measured results of those filters agree very well. The bandwidth of the first band in the developed filters extends from 1.75 GHz to 3.75 GHz with less than 0.3 dB insertion loss at the center of the band. The second band has a bandwidth that extends from 6.95 GHz to 8.75 GHz with less than 0.5 dB insertion loss at the center of that band. The stopband separating those two passband has more than 30 dB attenuation with transmission zero at 5.85 GHz.

1. INTRODUCTION

With the huge and fast developments in wireless communications, the design of many passive circuits, such as bandpass filters, faces new challenges including the requirements for a compact size, wide bandwidth and multi-band operation. The high data-rate wireless communication systems require wide bandwidth up to several hundreds of megahertz and the flexibility to operate at multiple frequency bands.

Received 4 November 2012, Accepted 1 December 2012, Scheduled 4 December 2012

* Corresponding author: Jayaseelan Marimuthu (j.marimuthu@uq.edu.au).

The design of dual-band filters at microwave frequencies is still challenging since it has to take into consideration many parameters, such as the center frequency, bandwidth and passband functions at the multiple passbands. There have been many innovative dual-band bandpass filter designs [1–16]. The proposed filters are based on uniform impedance resonators UIR [1], split ring step impedance resonators SIR [2], cross-coupled structure on low temperature co-fired ceramic [3], SIRs in vertical-stacked parallel-coupled configuration [4], radial SIRs with variable impedance ratio [5], and meander-loop resonator [6, 7]. In other methods, dual-band bandpass filters are designed using folded SIRs [8], multilayer coupled structure [9], asymmetric SIR [10], half-wavelength SIRs [11, 12], stub-loaded SIR [13], trisection SIRs [14], and coupled three-line resonators [15].

Parallel coupled microstrip lines (PCML) have been used as coupling components in various designs of bandpass filters [15, 16]. For a broadband performance, the PCML structure is required to be tightly coupled. This requirement can be realized if narrow lines and gap, and slotted ground structures are utilized. However, this option is not preferred due to the manufacturing difficulty of those narrow structures.

A stepped impedance resonator (SIR) combined with PCML is suitable for the filter design because the higher order resonant modes can be shifted or suppressed, and the spurious frequency response can be used to create a second passband for a dual-passband response [2, 4, 12]. The first and second passband responses are achieved by using appropriate impedance ratio and coupling of the utilized structure.

In this paper, a dual-band broadband bandpass with a pair of high coupled PCML-SIR structure with a central microstrip resonator is proposed based on the method presented in [17]. The enhancement of PCML structure tight coupling over the wide frequency range and dual-band is realized by using a feeding network with lower impedance. The PCML structure's coupling characteristics and dual-band depends on the dimensions of the feeding network. The novelty of this design is in using low impedance resonators to replace the feeding networks at the input and output port. The aim of using those resonators is to improve the coupling performance of the PCML structure across the required dual bands compared with the conventional method where the dimensions of the PCML are used to control the coupling factor, and the overall performance.

The dimensions of the central microstrip resonator and PCML-SIR are adjusted to improve the insertion loss, return loss, harmonic suppression and bandwidth at both bands. The widths of the middle

resonator and PCML-SIR are adjusted to improve the insertion loss and return loss performance of the dual passband response, while the length of the middle resonator is adjusted for the harmonic cancellation by creating and changing the position of the transmission zero frequency. The impedance ratio and the length ratio of PCML-SIR are mainly used to control the bandwidth of both bands. The design also has a transmission zero that is used to isolate both bands effectively. The details of the dual broadband filter design are presented and the measured results are given to demonstrate its performance.

2. SINGLE STAGE PCML-SIR STRUCTURE

A single stage PCML-SIR structure is shown in Fig. 1(a). It is used to investigate the effect of varying the impedance ratio on the dual band performance. The physical parameters of PCML strip and slots widths are $w_1 = 0.6\,\text{mm}$, $s_1 = 0.2\,\text{mm}$ and the length $l_1 = 14\,\text{mm}$ ($\approx \lambda/4$ at 2.65 GHz). Those dimensions give the following values for the odd-mode and even-mode impedances; $Z_{\text{odd}} = 45.778\,\Omega$ and $Z_{\text{even}} = 116.832\,\Omega$. As depicted in Fig. 1(a), a low impedance rectangular resonator with length $l_f = 4\,\text{mm}$ and a width w_f that is adjusted to change the impedance and thus to investigate the overall coupling factor at the two bands. The design is constructed on a substrate with a relative permitivity $\varepsilon_r = 6.15$ and thickness $h = 1.27\,\text{mm}$.

Since the PCML-SIR structure given in Fig. 1(a) is reciprocal and lossless, an equivalent circuit as shown in Fig. 1(b) can be obtained based on PCML-SIR two port network admittance, with $B_a = B_{11} + B_{12}$ and $B_b = -B_{12}$. $B_{11} = B_{22}$ and $B_{12} = B_{21}$ are the two independent susceptances of relevant admittance (Y) matrix of Fig. 1(a). Fig. 1(c), shows the equivalent circuit of PCML-SIR based on Fig. 1(b), where the PCML-SIR is modeled as a J-inverter network with susceptance (J) at the center and two equal electrical lengths ($\theta/2$) at the two sides [18].

For the PCML-SIR depicted in Fig. 1(a), the characteristics impedances of (Z_{even}, Z_{odd}), phase constants (β_{even}, β_{odd}) and lengths (l_{even}, l_{odd}) at the even- and odd-modes allow deriving the two port admittance (Y) matrix [19] as follows:

$$Y_{11} = Y_{22} = \frac{-j}{2}\left[\frac{1}{Z_{\text{even}}}\cot\beta_{\text{even}}l_{\text{even}} + \frac{1}{Z_{\text{odd}}}\cot\beta_{\text{odd}}l_{\text{odd}}\right] \quad (1)$$

$$Y_{12} = Y_{21} = \frac{-j}{2}\left[\frac{-1}{Z_{\text{even}}}\csc\beta_{\text{even}}l_{\text{even}} + \frac{1}{Z_{\text{odd}}}\csc\beta_{\text{odd}}l_{\text{odd}}\right] \quad (2)$$

Equations (1) and (2) imply that each element in the Y-matrix is

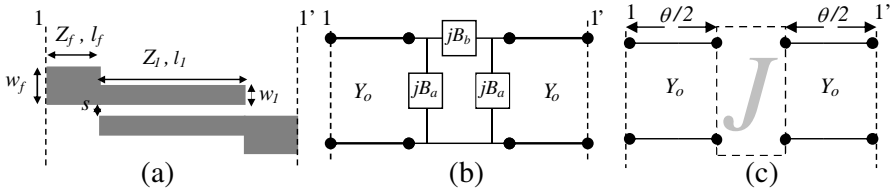

Figure 1. (a) Single stage PCML-SIR structure, (b) equivalent circuits for reciprocal two port network admittance for lossless PCML-SIR structure, (c) equivalent J-inverter network with susceptance J of PCML-SIR structure.

purely imaginary for PCML-SIR structure with the two independent susceptances of $B_{11} = B_{22}$ and $B_{12} = B_{21}$. The Z_{even}, Z_{odd}, β_{even}, β_{odd}, l_{even} and l_{odd} as given in Equations (1), (2) are the parameters of the PCML-SIR structure as shown in Fig. 1(a).

The two–port admittance Y-matrix of PCML-SIR as shown in Fig. 1(a) is extracted by using the commercial electromagnetic software Sonnet. Based on the extracted Y-matrix of the two port PCML-SIR, the susceptances $B_{11} = B_{22}$ and $B_{12} = B_{21}$ are used to calculate the normalized J-susceptance ($\bar{J}$) and electrical length (θ) as shown below [20].

$$\bar{J} = \left|\tan\left(-\frac{\theta}{2} + \theta_{\text{add}}\right)\right| \tag{3}$$

$$\theta = [\theta_{\text{sub}} + \theta_{\text{add}}] \tag{4}$$

$$\theta_{\text{add}} = n\pi + \left[\tan^{-1}\left(\frac{B_{11}}{Y_O} + \frac{B_{12}}{Y_O}\right)\right] \tag{5}$$

$$\theta_{\text{sub}} = n\pi + \left[\tan^{-1}\left(\frac{B_{11}}{Y_O} - \frac{B_{12}}{Y_O}\right)\right] \tag{6}$$

$$n = 0,\ 1,\ 2,\ 3\ldots$$

$n = 0, 1, 2\ldots$, and $Y_o = 1/(Z_o = 50\,\Omega)$ is the characteristic admittance of the uniform lines that excite the open-circuited PCML at the two sides.

Figure 2(a) shows the normalized J-inverter susceptance ($\bar{J}$) of the PCML-SIR structure, with various resonators width w_f which calculated based on Equations (3)–(6) as explained above. It shows that as w_f increases from 1.9 mm ($Z_f = 49.5\,\Omega$) to 2.9 mm ($Z_f = 38.3\,\Omega$), the $\bar{J}$ peak value for both bands increases as well. The second band centered at 7.85 GHz ($\bar{J}$ peak value is from 0.73 to 1.18) increases at a higher rate compared to the first band centered at 2.65 GHz ($\bar{J}$ peak value is from 0.71 to 0.88). By looking into the J-inverter network

of Fig. 1(c) for PCML-SIR structure, the reflection coefficient can be written as:

$$S_{11} = \frac{1 \;\; \bar{J}^{\,2}}{1 + \bar{J}^{\,2}} \tag{7}$$

It clearly shows that $S_{11} = 0$ when $\bar{J} = 1$. The frequency of $\bar{J} = 1$ corresponds to the S_{11} pole location over the bandpass range. Fig. 2(a) shows the S-parameters that the S_{11} pole appears at the same frequency when $\bar{J} = 1$ based on Equation (7). For PCML-SIR with $w_f = 2.9\,\text{mm}$ ($Z_f = 38.3\,\Omega$), the corresponding S_{11} poles appear at the two frequencies 7.3 GHz and 8.0 GHz of the second band when $\bar{J} = 1$.

The above PCML-SIR structure also produces transmission zero at 5.85 GHz within the stopband which isolating both bands effectively. The length of PCML structure chosen to be $l_1 = 14\,\text{mm}$ ($\approx \lambda/4$ at 2.65 GHz and $\approx 3\lambda/4$ at 7.85 GHz) to ensure the transmission zero of PCML-SIR appear between 2.65 GHz and 7.85 GHz based on Equation (8) [21].

$$\frac{Z_{\text{odd}}}{Z_{\text{even}}} = \frac{\sin\left(\beta_{\text{odd}} l_{\text{odd}}\right)}{\sin(\beta_{\text{even}} l_{\text{even}})} \tag{8}$$

Equation (8) derived from PCML-SIR structure two-port Z-parameters enforces $Z_{21} = 0$ or $S_{21} = 0$ for a transmission zero. For the above condition at 5.85 GHz the $Z_{\text{odd}} = 45.272\,\Omega$, $Z_{\text{even}} = 117.829\,\Omega$, $\beta_{\text{odd}} = 0.233\,\text{rad/mm}$ and $\beta_{\text{even}} = 0.26\,\text{rad/mm}$. Based on Equation (8), the transmissions zero of PCML-SIR structure depend on the resonator length of PCML.

Figure 2(b) shows the $\bar{J}$ peak value for the first and second band as a function of the impedance ratio $k_{zo} = Z_f/Z_1$ with fixed $Z_1 = 73\,\Omega$, which is calculated using $Z_1 = \sqrt{Z_{\text{odd}} Z_{\text{even}}}$, and varies Z_f (34.55 Ω–84.3 Ω). It shows that the $\bar{J}$ peak value for both bands depends on the impedance ratio k_{zo} of the resonators. The $\bar{J}$ peak value for the respective bands varies at different rate as the impedance ratio k_{zo} increases and this can be divided in three cases ($k_{zo} > 0.69$, $k_{zo} = 0.69$ and $k_{zo} < 0.69$). For the first case when $k_{zo} > 0.69$ ($Z_f > 50\,\Omega$), both bands show low coupling factor with $\bar{J} < 0.69$ with flat reducing response for band 1 and fast reducing response for band 2 as k_{zo} increases. Since the insertion and return losses for both bands at this condition are low, this case is not suitable for dual-band applications due to the low bandwidth at the two bands.

For the second case when $k_{zo} = 0.69$ ($Z_f = 50\,\Omega$), both bands show the same coupling factor with $\bar{J} = 0.69$. Since the insertion, return loss and bandwidth for the two bands are low; this case is not suitable for dual band applications.

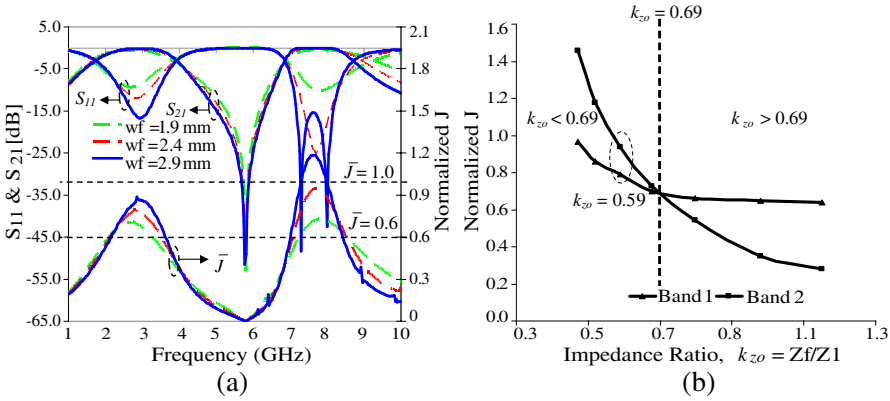

Figure 2. (a) PCML-SIR S-parameters and normalized $\bar{J}$ susceptances, and (b) PCML-SIR normalized $\bar{J}$ susceptances vs. impedance ratio.

For the third case when $k_{zo} < 0.69$ ($Z_f < 50\,\Omega$), the coupling factor for both bands is excellent and shows that $\bar{J} > 0.69$ as k_{zo} is reduced. The coupling factor at band 2 is larger and increasing at higher rate as k_{zo} is reduced compared with the value at band 1. As k_{zo} is reduced, the insertion and return losses for the two bands show excellent performance. This case is suitable for the dual-band design as both bands have a suitable bandwidth. For a dual-band design, the PCML structure with $k_{zo} = 0.59$ is selected. In this case, $w_f = 2.4\,\text{mm}$ ($Z_f = 43.2\,\Omega$) and $w_1 = 0.6\,\text{mm}$ ($Z_1 = 73\,\Omega$) with $\bar{J} = 0.792$ at band 1 and $\bar{J} = 0.938$ band 2. At the selected value for k_{zo}, Fig. 2(a) shows that the two bands have good insertion loss and return loss with preferred bandwidths for dual-band applications.

Although the coupling shows better performance when $k_{zo} < 0.59$, this is not a preferred design case because high/over coupling at band 2 causes a drop in insertion loss at the center frequency of band 2.

3. PROPOSED DUAL-BAND BANDPASS FILTER

The prototype layout of the proposed dual broadband filter is shown in Fig. 3. The PCML-SIR strip and slot widths are set as given in the analysis presented earlierin order to achieve a dual broad operation with tight coupling and relaxed fabrication tolerance. Meanwhile, the middle resonator is formed with length l_2 and width w_2 in order to achieve a length of slightly greater than $\lambda/4$ at 2.65 GHz. The feeding network of width $w_f = 1.9\,\text{mm}$ ($Z_f = 49.5\,\Omega$) and length $l_f = 4\,\text{mm}$

for the input and output port is utilized.

Figure 4 shows the simulated results of S_{11} and S_{21} of the dual broadband filter over the wide frequency range (1–10 GHz) with respect to the different middle resonator widths (Fig. 4(a)) and lengths (Fig. 4(b)). Six resonant frequencies are present within the investigated band with a transmission zero at 5.85 GHz. The first (f_1) and second (f_2) resonant frequencies form the first operational band (band 1), whereas the forth (f_4) and fifth (f_5) resonant frequencies form the second operational band (band 2). The third (f_3) and sixth (f_6) resonant frequencies represent the undesired harmonic frequencies. The position of the resonant frequencies and the insertion and return loss within the passbands of band 1 and band 2 depend on the length (l_2) and the width (w_2) of the middle resonator.

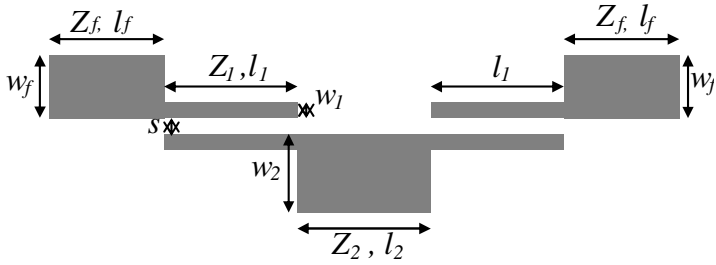

Figure 3. Proposed dual-band broadband BPF.

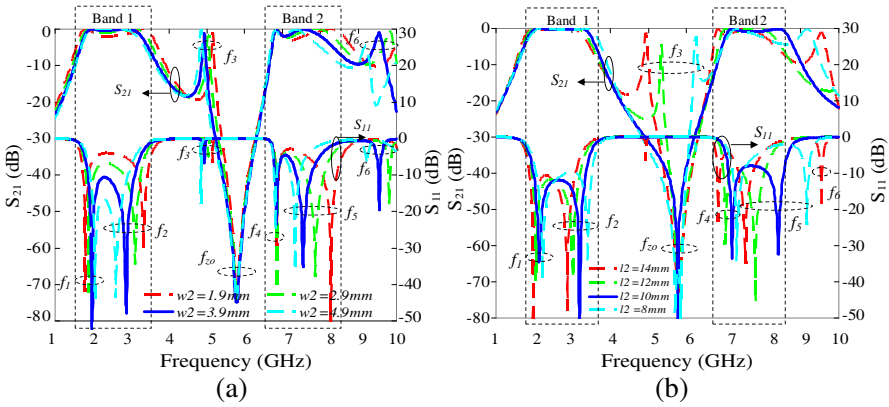

Figure 4. Predicted S-parameters (a) for various widths of w_2 and fixed $l_2 = 14$ mm, and (b) for various lengths of l_2 and fixed $w_2 = 3.9$ mm.

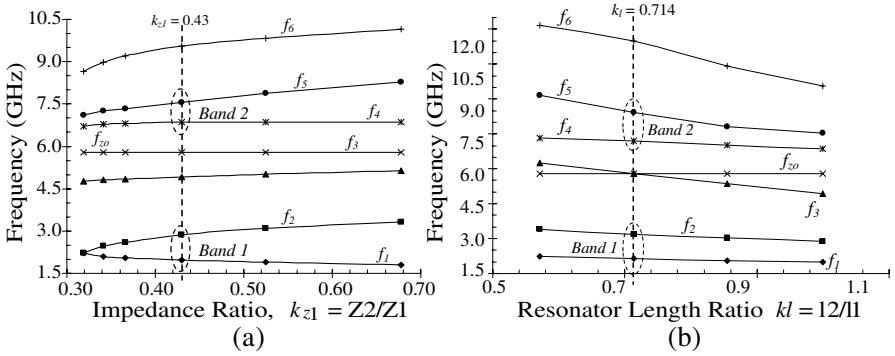

Figure 5. Predicted dual broadband bandpass filter performance. (a) Resonant frequency vs impedance ratio, and (b) resonant frequency vs length Ratio.

Figure 5(a) shows the effect of various resonant frequencies with respect to the impedance ratio $k_{z1} = Z_2/Z_1$ for a fixed $Z_1 = 73\,\Omega$ and variable Z_2 (from $23.3\,\Omega$ to $49.5\,\Omega$). It shows that as k_{z1} decreases, the resonant frequencies of the first and second band get closer to each other and the operating bandwidths of those bands are reduced. For band 1, when $k_{z1} = 0.32$ ($Z_2 = 23.3\,\Omega$), the resonant frequencies $f_1 = f_2$, and overall bandwidth of the respective band become very small.

The first (f_3) and second (f_6) harmonic frequencies are further reduced and brought nearer to the operating band of the filter if k_{z1} is reduced. There is no sign of suppression of any of them by the transmission zero frequency (f_{zo}). For a reasonable dual band operation, $k_{z1} = 0.43$ is selected with $w_2 = 3.9\,\text{mm}$ ($Z_2 = 31.4\,\Omega$). This value guarantees a realizable separation between the resonant frequencies of the two bands with very small insertion losses.

Figure 5(b) shows the effect of the resonator's length ratio $k_l = l_2/l_1$ (fixed $l_1 = 14\,\text{mm}$ and variable l_2 from 8 mm to 14 mm) on the resonant frequencies. It shows that as k_l decreases, the resonant frequencies of the first and second bands are further separated from each other and the overall operating bandwidth is improved. The first (f_3) and second (f_6) harmonics frequencies increase and the first (f_3) harmonic frequency is suppressed by the transmission zero frequency (f_{zo}) when $k_l = 0.714$. At the same time, the second (f_6) harmonic frequency is shifted away from the operating band. For a reasonable dual band operation with harmonic suppression, $k_l = 0.714$ is selected with $l_2 = 10\,\text{mm}$ which slightly shorter than the coupled line. This is due to at both end of low impedance middle resonator which has

step in line width, the stray capacitance exists and giving an effective increased of the length.

The performance of the final structure with $w_f = 1.9\,\text{mm}$, $l_f = 4.0\,\text{mm}$, $w_1 = 0.6\,\text{mm}$, $l_1 = 14.0\,\text{mm}$, $s = 0.2\,\text{mm}$, $w_2 = 3.9\,\text{mm}$ and $l_2 = 10\,\text{mm}$ is simulated and included in Fig. 4(b). The performance of the final design indicates a significant improvement in the insertion loss and return loss of the second band and able to remove harmonic frequency (f_3) significantly.

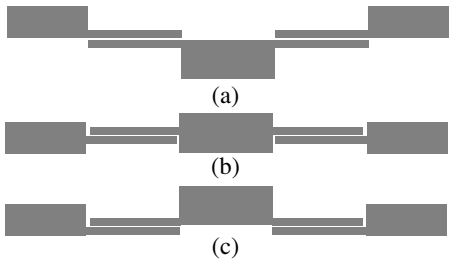

Figure 6. The three designed prototypes with different edge capacitive coupling.

Table 1. Optimized design parameters for the filters.

Design	w_f (mm)	l_f (mm)	w_1 (mm)	l_1 (mm)	s (mm)	w_2 (mm)	l_2 (mm)
Design (a)	2.4	4.0	0.6	14	0.2	3.9	10.0
Design (b)	1.9	4.0	0.6	14	0.2	3.3	11.7
Design (c)	2.4	4.0	0.6	14	0.2	4.9	10.7

Table 2. Summary of measured results of optimized filters.

Design	Band 1 @ 2.65 GHz			Band 2 @ 7.85 GHz		
	BW GHz	$\|S_{11}\|$ dB	$\|S_{21}\|$ dB	BW GHz	$\|S_{11}\|$ dB	$\|S_{21}\|$ dB
Design (a)	1.8 (68%)	< -12	> -0.3	1.8 (23%)	< -10	> -0.7
Design (b)	1.9 (72%)	< -30	> -0.2	1.9 (24%)	< -20	> -0.2
Design (c)	1.65 (62%)	< -20	> -0.2	1.4 (18%)	< -14	> -0.4

4. RESULTS AND DISCUSSIONS

Based on above investigation, three prototypes design as shown in Fig. 6 with different positions for the middle resonator are designed and optimized by using Agilent ADS Momentum. The optimized parameters obtained for the best possible performance concerning the insertion and return losses at in-band and out-band frequencies and also for relaxed fabrication tolerances are listed in Table 1. The optimized designs based on Table 1 are fabricated using RT/Duroid substrate of thickness of 1.27 mm with dielectric constants of 6.15. The performances of the fabricated filters are measured by using Agilent E5071C ATO 79866 network analyzer.

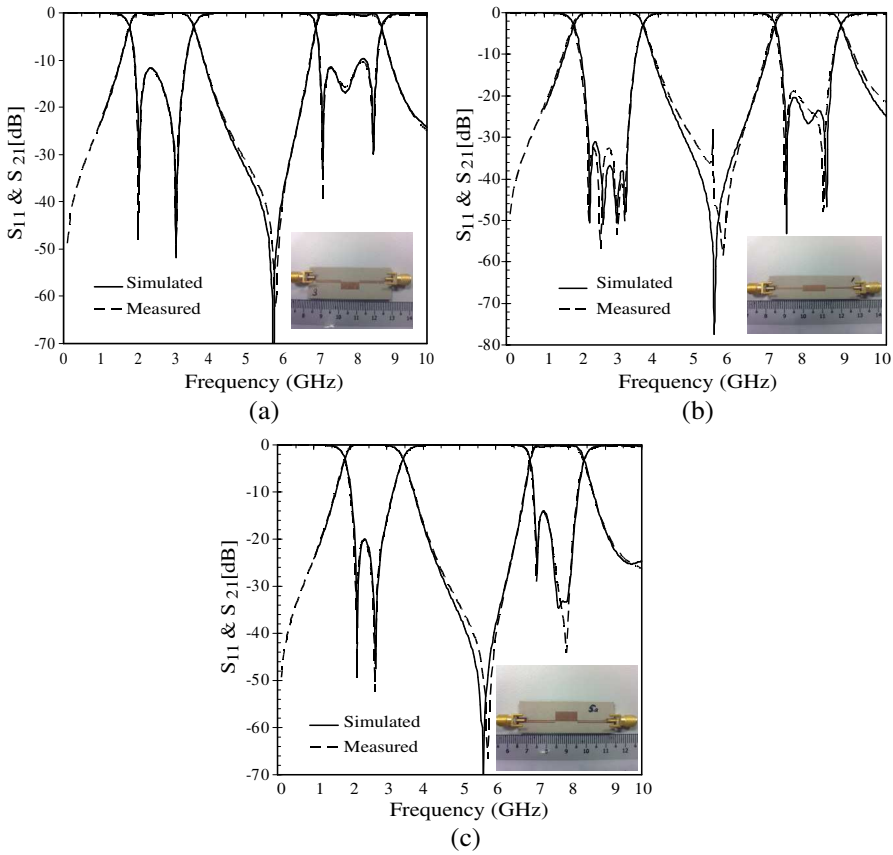

Figure 7. Simulated and measured S-parameters of optimized dual-band broadband filters with different configurations.

Figure 7 illustrates the simulated and measured S-parameters of the three optimized dual broadband filters. The measured and simulated results are found to have reasonably good agreement with each other. The result shows the possibility of changing the dimensions of the middle resonator and the effect of edge coupling to change the performance and bandwidths of the dual bands.

The optimized designs show excellent dual broadband characteristics. The presented results in Table 2 indicate that the proposed dual-band filters have broadband performance with excellent passband response using low cost structures. Table 2 shows that design (b) has excellent performance in regard to the insertion, return loss and bandwidth for both bands compared to design (a) and design (c). Meanwhile, design (c) shows improved performance compared to design (a). Design (b) and design (c) show an improvement in insertion and return loss mainly due to the edge coupling which is present due to the configuration of the structure. Comparatively, design (b) with double edge coupling shows better performance compared to design (c) with only single edge coupling and design (a) without any edge coupling.

5. CONCLUSION

A dual-band broadband bandpass filter has been presented. It uses a combination of parallel-coupled microstrip lines and stepped impedance resonators. To improve the performance at the dual bands, additional low impedance resonators are used at the input and output feeding networks to enhance the coupling factor at both bands. The dimensions of the central resonator are used to control the width and position of the two bands. The simulated and measured results of three developed prototypes show an excellent dual broadband bandpass performance.

REFERENCES

1. Yang, R.-Y., H. Kuan, C.-Y. Hung, and C.-S. Ye, "Design of dual-band bandpass filters using a dual feeding structure and embedded uniform impedance resonators," *Progress In Electromagnetics Research*, Vol. 105, 93–102, 2010.
2. Xiao, J.-K. and H.-F. Huang, "New dual-band bandpass filter with compact sir structure," *Progress In Electromagnetics Research Letters*, Vol. 18, 125–134, 2010.
3. Chen, C., "Dual-band bandpass filter using coupled resonator pairs," *IEEE Microwave and Wireless Components Letters*, Vol. 15, No. 4, 259–261, 2005.

4. Kuo, J., T. Yeh, and C. Yeh, "Design of microstrip bandpass filters with a dual-passband response," *IEEE Trans. Microwave Theory Tech.*, Vol. 53, No. 4, 1331–1337, 2005.
5. Wang, J., Y. Guo, B. Wang, L. Ong, and S. Xiao, "High-selectivity dual-band stepped-impedance bandpass filter," *Electronics Letters*, Vol. 42, No. 9, 2006.
6. Hu, X., Q. Zhang, and S. He, "Compact dual-band rejection filter based on complementary meander line split ring resonator," *Progress In Electromagnetics Research Letters*, Vol. 8, 181–190, 2009.
7. Wu, G.-L., W. Mu, X.-W. Dai, and Y.-C. Jiao, "Design of novel dual-band bandpass filter with microstrip meander-loop resonator and CSRR DGS," *Progress In Electromagnetics Research*, Vol. 78, 17–24, 2008.
8. Mokhtaari, M., J. Bornemann, and S. Amari, "Quasi-elliptic dual-band filter design using stepped-impedance resonators and coupling topologies for narrow-to-wide-band applications," *IET Microwave Antenna Propag.*, Vol. 2, No. 8, 863–870, 2008.
9. Djoumessi, E. and K. Wu, "Multilayer dual-mode dual-bandpass filter," *IEEE Microwave and Wireless Components Letters*, Vol. 19, No. 1, 21–23, 2009.
10. Zhang, X., J. Chen, J. Shi, and Q. Xue, "High-selectivity dual-band bandpass filter using asymmetric stepped-impedance resonators," *Electronics Letters,* Vol. 45, No. 1, 2009.
11. Shi, J. and Q. Xue, "Dual-band and wide-stopband single-band balanced bandpass filters with high selectivity and common-mode suppression," *IEEE Trans. Microwave Theory Tech.*, Vol. 58, No. 8, 2204–2212, 2010.
12. Jiang, M., L. Chang, and A. Chin, "Design of dual-passband microstrip bandpass filters with multi-spurious suppression," *IEEE Microwave and Wireless Components Letters*, Vol. 20, No. 4, 199–201, 2010.
13. Velazquez-Ahumada, M. D. C., J. Martel-Villagr, F. Medina, and F. Mesa, "Application of stub loaded folded stepped impedance resonators to dual band filters," *Progress In Electromagnetics Research*, Vol. 102, 107–124, 2010.
14. Ma, D.-C., Z.-Y. Xiao, L.-L. Xiang, X.-H. Wu, C.-Y. Huang, and X. Kou, "Compact dual-band bandpass filter using folded SIR with two stubs for WLAN," *Progress In Electromagnetics Research*, Vol. 117, 357–364, 2011.
15. Kuo, J.-T., C.-Y. Fan, and S.-C. Tang, "Dual-wideband bandpass

filters with extended stopband based on coupled-line and coupled three-line resonators," *Progress In Electromagnetics Research*, Vol. 124, 1–15, 2012.

16. Zhu, L., S. Sun, and W. Menzel, "Ultra-wideband (UWB) bandpass filters using multiple-mode resonator" *IEEE Microwave and Wireless Components Letters*, Vol. 15, No. 11, 2005.
17. Marimuthu, J. and M. Esa, "Three element compact broadband parallel-coupled microstrip bandpass filter of simple configuration," *IEEE Proc. of Asia-Pacific Conference on Applied Electromagnetics*, Melaka, Malaysia, Dec. 2007.
18. Hong, J. S. and M. J. Lancaster, *Microstrip Filters for RF/Microwave Applications*, Wiley, New York, 2001.
19. Zysman, G. I. and A. K. Johnson, "Coupled transmission line networks in an inhomogeneous dielectric medium," *IEEE Trans. Microwave Theory Tech.*, Vol. 17, No. 10, 1969.
20. Marimuthu, J. and M. Esa, "Equivalent J — Inverter network parameters analysis and cancellation of spurious response of parallel coupled microstrip line," *IEEE International RF and Microwave Conf.*, Kuala Lumpur, Malaysia, Dec. 2006.
21. Marimuthu, J. and M. Esa, "Experimental performance of harmonic suppressed bandpass filter," *IEEE Proc. of Asia-Pacific Conference on Applied Electromagnetics*, Melaka, Malaysia, Dec. 2007.